

Vacancy Defects in Silicon Related
Materials and Gallium Nitride

Mikko Rummukainen

*Laboratory of Physics
Helsinki University of Technology
Espoo, Finland*

Dissertation for the degree of Doctor of Science in Technology to be presented with due permission of the Department of Engineering Physics and Mathematics for public examination and debate in Auditorium K at Helsinki University of Technology (Espoo, Finland) on the 12th of January, 2007, at 13 o'clock.

Dissertations of Laboratory of Physics, Helsinki University of Technology
ISSN 1455-1802

Dissertation 144 (2007):

Mikko Rummukainen: Vacancy Defects in Silicon Related Materials and Gallium Nitride

ISBN 978-951-22-8571-6 (print)

ISBN 978-951-22-8572-3 (electronic)

Otamedia OY
ESPOO 2007

Abstract

Defects on the atomic scale strongly affect the performance of semiconductor devices and the achievable device lifetimes. Positron annihilation spectroscopy is sensitive to vacancy-type defects, which are the most common type of structural defects. In this thesis positron annihilation spectroscopy has been applied to study vacancy defects in gallium nitride and silicon related materials: silicon, silicon germanium and germanium.

Silicon related materials are dominant in current integrated circuits. Improving the channel conductivity is crucial for reducing the heat dissipation and for production of faster components. The formation of compensating defect complexes has been observed and their structure identified in highly Sb doped silicon. Native point defects in silicon germanium have been studied for Ge concentrations up to 30 per cent. Vacancies are found to form pairs with dopant P atoms reducing the free electron density and therefore the conductivity. In germanium implanted with silicon and germanium ions vacancy clustering and defect recovery during heat treatment were studied.

Gallium nitride is the most common material for blue light emitting diodes (LEDs). Blue wavelength light is required for producing e.g. high intensity white LEDs and improving the data packing density of DVDs. Bulk GaN is expensive and not readily available. Therefore GaN components are grown as thin layers on foreign substrates, the properties of which affect the GaN layer. The dislocation density was observed to decrease when using misoriented SiC substrates. The vacancy formation and impurity incorporation into GaN layers was shown to be dependent on the growth polarity. Vacancy clusters and a higher concentration of impurities are incorporated during N-polar growth.

Tiivistelmä

Atomiskaalan virheet vaikuttavat ratkaisevasti puolijohdekomponenttien suorituskykyyn ja laitteiden kestävyYTEEN. Positroniannihilaatiospektroskopia on erinomainen menetelmä tutkittaessa vakanssityypisiä virheitä, jotka ovat tyypillisimpiä pistemäisiä virheitä. Tässä työssä positroniannihilaatiospektroskopiaa on hyödynnetty galliumnitridin ja piintyyppisten materiaalien - pii, piigermanium ja germanium - tutkimuksessa.

Suurin osa integroiduista piireistä valmistetaan piintyyppisistä materiaaleista. Materiaalin johtavuuden parantaminen on avainasemassa pyrittäessä pienentämään lämmöntuottoa ja valmistamaan entistä nopeampia komponentteja. Tässä työssä on havaittu ja tunnistettu johtavuutta heikentäviä virhekertymiä vahvasti antimonilla seostetussa piissä. Luonnostaan piigermaniumissa esiintyviä virheitä on tutkittu materiaaleissa, joissa germaniumin osuus on 0 - 30 %. Vakanssien on havaittu kertyvän seostuksessa käytettyjen fosforiatomien ympärille vähentäen elektronitiheyttä ja siten johtavuutta. Germaniumissa, jota on säteilytetty piillä tai germaniumilla, vakanssien kertymistä ryppäiksi ja ryppäiden poistumista lämpökäsittelyn avulla on tutkittu.

Galliumnitridi on yleisimmin käytetty materiaali sinisissä valoa emittoivissa diodeissa (LED). Sinistä valoa tarvitaan mm. tuottamaan kirkkaita valkoisia LED valoja sekä parantamaan tiedon tallennustiheyttä DVD levyillä. Yksittäiskiteinen GaN on erittäin kallista ja sen saatavuus on heikko. Siksi GaN komponentteja kasvatetaan ohuina kalvoina vieraiden aineiden pinnalle, jolloin alustan ominaisuudet vaikuttavat kerrokseen. Tässä työssä on havaittu dislokaatiotiheyden kasvavan, kun kerros kasvatetaan piikarbidialustoille, joiden kidesuunta ei ole leikkauspinnan suuntainen. Vakanssivirheiden synnyn ja epäpuhtausatomien kertymisen on osoitettu riippuvan GaN:n kasvusuunnasta. Epäpuhtausatomit sitoutuvat paremmin ja kasvatuksessa muodostuu enemmän vakanssirypäitä, kun GaN kide kasvatetaan N-polaarisesti.

Preface

This thesis has been prepared in the Positron Group of the Laboratory of Physics at the Helsinki University of Technology during the years 2003–2006. I am grateful to Prof. Pekka Hautojärvi for giving me the opportunity to work in the positron group.

I am indebted to the late Prof. Kimmo Saarinen for the excellent guidance and supervision he could provide me for the vast majority of time I was working in the laboratory. This thesis wouldn't exist without his enthusiasm and creativity. I am also glad for help and insight of Dr. Klaus Rytsölä and the skillful people at the electronic and mechanical workshops. I am also grateful for Prof. Martti Puska and M.Sc. Ilja Makkonen for providing us with theoretical results and improving our theoretical understanding.

I wish to thank the members of the positron group, both current and former, for creating a pleasant and inspiring working environment. My colleagues were ever ready to help in problems ranging from positron physics to world politics.

I wish to thank my parents, sisters and friends for all the support, encouragement and joy they have provided during the years. Also, I wish to thank August Associates for giving me the time needed to finish this thesis. Finally, I wish to thank my wife Taru for supporting me and helping us to construct our future together.

Helsinki, December 2006

Mikko Rummukainen

Contents

Abstract	i
Tiivistelmä	ii
Preface	iii
Contents	iv
List of publications	v
1 Introduction	1
2 Positron Annihilation Spectroscopy	4
2.1 Positron beams	4
2.2 Doppler-broadening experiments	5
2.3 Data analysis	6
3 Defects in Silicon Related Materials	10
3.1 Highly doped silicon	11
3.2 Silicon germanium	15
3.3 Germanium	18
4 Defects in Gallium Nitride	21
4.1 SiC as substrate material	22
4.2 Growth polarity	25
5 Summary	29

List of publications

This thesis consists of an overview and the following publications:

- I** M. Rummukainen, I. Makkonen, V. Ranki, M. J. Puska, K. Saarinen and H.-J. L. Gossmann, *Vacancy-Impurity Complexes in Highly Sb-Doped Si Grown by Molecular Beam Epitaxy*, Physical Review Letters **94**, 165501:1-4 (2005).
- II** M. Rummukainen, J. Slotte, K. Saarinen, H. H. Radamson, J. Hållsted and A. Yu. Kuznetsov, *Vacancy-impurity pairs in relaxed $Si_{1-x}Ge_x$ layers studied by positron annihilation spectroscopy*, Physical Review B **73**, 165209:1-8 (2006).
- III** M. Rummukainen, J. Slotte, F. Tuomisto, V. Markevich and A. R. Peaker, *Radiation damage in ion implanted and annealed n-type Ge studied by positron annihilation spectroscopy*, Helsinki University of Technology Publications in Engineering Physics, Report TKK-F-A845 (2006).
- IV** E. Tengborn, M. Rummukainen, F. Tuomisto, K. Saarinen, M. Rudzinski, P. R. Hageman, P. K. Larsen and A. Nordlund, *Effect of the misorientation of the 4H-SiC substrate on the open volume defects in GaN grown by metal-organic chemical vapor deposition*, Applied Physics Letters **89**, 091905:1-3 (2006).
- V** M. Rummukainen, J. Oila, A. Laakso, K. Saarinen, A. J. Ptak and T. H. Myers, *Vacancy Defects in O-doped GaN Grown by Molecular Beam Epitaxy: The Role of Growth Polarity and Stoichiometry*, Applied Physics Letters **84**, 4887-4889 (2004).

The author has had an active role in all the phases of the research reported in this thesis. He has participated actively in the development and construction of the measurement instruments, planning and performing the experiments, analysis of the experimental data, and he has contributed significantly to the interpretation of the results. The analysis of all the positron data has been made by the author. The theoretical calculations have been made by the author excluding those of Publication I. The author has written Publications I - III and V. The work in Publication IV was performed under the author's guidance.

Chapter 1

Introduction

Semiconductors are the basis of modern electronics and optoelectronics. The electrical conductivity of these materials can be changed over several orders of magnitude by controlled addition of impurity atoms to the lattice. The charge carriers may be either negatively (electrons) or positively charged (holes). The majority charge carriers are negative in an *n*-type material and positive in a *p*-type material. Many semiconductor materials are suitable for optoelectronic devices due to the direct forbidden energy gap in the 1.5 - 3 eV range required for optic transitions. [1–3]

Silicon is the most common semiconductor material used in current integrated circuits. It has been possible to increase the computing speed of microprocessors by manufacturing smaller and smaller Si field-effect transistors (FETs) which act as the basic logical elements of the device. The decrease of the size of the FET requires an increase in the conductivity of the source and drain electrodes as well as in the channel. When Si is doped to concentrations above $\approx 3 \times 10^{20} \text{ cm}^{-3}$ fundamental material problems start to appear and the charge carrier concentration does not increase any more. The problem can be overcome by adding germanium atoms to the FET or using strained structures where the conductivity is higher. It is also possible to grow the material at low temperatures where the dopant atoms remain electrically active despite the high doping density because the dopant atoms do not have time to reach thermodynamical equilibrium during growth. [1]

Light emitting diodes (LEDs) are much more efficient than conventional light bulbs for converting energy into light. In order to produce white light, different wavelengths of light, including blue light, have to be present. Laser LEDs in the blue and ultraviolet region can be used to store data more densely on DVDs due to their shorter wavelength, as in the recent BlueRay DVD players. For the

semiconductor LEDs to emit light in the blue to UV spectral region, materials with a wide band gap of approximately 3 eV are needed. [2]

Lattice imperfections are a critical issue for understanding the properties of the material. The most common type of imperfections are point-like defects, which include both intentional and unintentional impurities and intrinsic point defects such as vacancies and interstitials. The formation of point defects in semiconductor materials is governed by both the thermodynamics and the kinetics during growth, processing and cooling phases. The stability of a defect is important, since often point defects are mobile at typical processing temperatures of several hundred degrees Celsius. In order to produce materials of high quality, it is imperative to control the formation of the point defects and understand how post-growth processing affects them. [3]

In this thesis positron annihilation spectroscopy (PAS) was applied to study open volume defects in gallium nitride and modern silicon related materials. PAS is a powerful tool providing unambiguous identification of vacancy-type defects. It gives information on the atomic structure, charge state and concentration of the defects.

In Publications I and II, we have studied complexing of vacancies with dopant atoms in *n*-type silicon and silicon germanium (SiGe). Our PAS measurements, supported by theoretical predictions, show the formation of metastable vacancies and vacancy clusters in highly Sb-doped Si grown at low temperatures. The open-volume defects are neighbored by 1-2 Sb impurity atoms, and their concentration is large enough to be important for the electrical deactivation of the Sb doping. In SiGe we observe pairing of vacancies with the dopant P atoms. The Ge concentration around the vacancy phosphorus pair is the same as in the surrounding lattice and no Ge clustering around the vacancy was observed.

In Publication III we have studied ion implantation damage in germanium. Ion implantation is used for processing semiconductor materials. The implantation ions generate high concentrations of defects and at the highest studied fluences they amorphize the material. Heat treatment of the implanted material leads at first to vacancy clustering and at high enough temperatures the material recrystallizes. The size of the vacancy clusters formed is larger and the temperature needed to remove the defects higher in material having more lattice damage.

In Publication IV we have studied the effect of substrate orientation on defect formation. In GaN grown on misoriented 4H-SiC substrates we observe simple vacancies and vacancy clusters for all substrate orientations. In addition to vacancies, positrons annihilate at shallow traps that are likely to be dislocations. The results show that the concentration of vacancy-type defects increases and the concentration of shallow positron traps decreases with the increasing substrate misorientation.

In Publication V we have studied defects in both Ga- and N-polar oxygen doped GaN. We have found that Ga-polar GaN is free of compensating Ga vacancies up to $[O]=10^{18} \text{ cm}^{-3}$ in Ga stable growth, but high concentrations of vacancies are formed in N-stable conditions. We also show that vacancy clusters are formed in N-polar material grown in Ga stable conditions, which may be related to the higher reactivity of the N-polar surface.

Chapter 2

Positron Annihilation Spectroscopy

Positron annihilation spectroscopy is an experimental method sensitive to negatively charged defects and defects with an open volume on the atomic scale. The method is based on the detection of the radiation produced in the annihilation of positrons (i.e. antiparticles of electrons) with electrons in a material. Usually in the annihilation event two photons are emitted in almost opposite directions with an energy near 511 keV. The momentum of the annihilating electron-positron pair is conserved in the process, and usually the momentum of the positron is small compared to that of the electron. The electron momentum causes Doppler-broadening of the 511 keV annihilation line.

Prior to annihilation, positrons can get trapped at vacancy type defects due to the missing Coulomb repulsion of the positive ion core. The electron momentum distribution in bulk material is different from the distribution in point defects. By measuring the Doppler-broadening it is possible to detect the presence of isolated missing atoms or the change of the atomic species of a single atom surrounding a vacancy. Thorough reviews on the measurement methods and the theory of positrons in solids can be found in Refs. [4–6].

2.1 Positron beams

Monoenergetic positron beams can be used to study thin semiconductor films. By varying the energy of the positrons it is possible to control the depth positrons probe in the sample allowing the measurement of defect profiles. Positrons are typically obtained from a radioactive ^{22}Na source, which emits positrons at energies

up to 544 keV. The positrons are first slowed down, moderated, and subsequently accelerated to the desired energy. In the equipment used in this study strong magnetic fields are used to guide the positrons from the source to the sample. The sample is located several meters from the source to minimize the background radiation from the source.

Positrons entering the sample lose their energy in processes like core-electron ionization and electron-hole excitation and phonon scattering. This thermalization process takes a few picoseconds. After thermalization the positron diffuses in the material, possibly gets trapped at a defect and finally annihilates with an electron. The diffusion length of the positrons varies with the material and the defect concentration. The diffusion length can range from tens of nanometers to several hundred nanometers. The achievable depth resolution is limited by the broadness of the positron implantation profile and the diffusion length.

2.2 Doppler-broadening experiments

In Doppler-broadening measurements one detects the broadening of the 511 keV annihilation line caused by the momentum of the annihilating positron-electron pair. The energy shift from 511 keV is $\pm \frac{1}{2}p_L c$, where p_L is the momentum of the annihilating pair in the direction of the annihilation photon and c is the speed of light. The annihilation photon energy E_γ is usually measured by a high-purity Ge-detector. The signal is amplified and fed into a digital stabilizer, which is used to remove the effect of instabilities in the measurement system. The pulses are collected to an energy histogram using a multichannel analyzer.

In order to characterize the Doppler spectrum shape parameters S and W are defined according to Fig. 2.1. The S parameter is defined as the number of counts in the center of the peak divided by the number of total counts in the peak. The S parameter thus characterizes the annihilation with the low momentum electrons, mainly valence electrons. Typically the S parameter is calculated at photon energies $|E_\gamma - 511 \text{ keV}| < 0.7 \text{ keV}$ corresponding to a momentum ($2.7 \times 10^{-3} m_0 c$), where m_0 is the rest mass of the positron. The W parameter is the fraction of counts in the wing region of the peak and characterizes annihilations with the high momentum electron, mainly core electrons. Energy windows used for the W parameter are usually between 2.5 keV ($10 \times 10^{-3} m_0 c$) and 7.0 keV ($27 \times 10^{-3} m_0 c$) from the peak center. Typically, positron trapping at vacancies increases the S parameter and decreases the W parameter. Impurities next to the vacancy may reduce or enhance the changes in the annihilation parameters.

The probability density of annihilation decreases with the increasing electron momentum. The background radiation therefore limits the accurate detection of

annihilations with high momentum electrons. It is possible to lower the level of background in the Doppler spectrum by using an additional efficient, low resolution detector for gating purposes and requiring the detection of both annihilation photons, as in Publication II. The annihilation event is recorded only if a signal is obtained from both the high resolution Ge-detector and the low resolution gate detector within a certain coincidence time. This way the background level can be reduced by a factor 100. [7, 8]

Even better results can be obtained by using two detectors with a high energy resolution, as in Publications I and III. The observed signals are placed into a two-dimensional matrix where the energies observed determine the column and row where the pulse is to be added (Fig. 2.1). Due to the conservation of momentum the annihilation events will be mainly on the diagonal of the 2D-spectrum, where $E_1 + E_2 = 2m_0c - E_b$, where E_b is the binding energy of the positron and the electron in the solid. Due to the finite resolution of the system counts where the sum of the photon energies are within 2 keV to $2m_0c$ are accepted to the final 1D spectrum. In addition to the very high peak-to-background ratio the resolution is improved by a factor of $\sqrt{2}$ in this system. Additionally, the resolution function of the system can be obtained from the other diagonal $E_1 - E_2 = \text{constant}$.

2.3 Data analysis

In real materials positrons annihilate in several different annihilation states e.g. the material surface, bulk material and different defects. The measured annihilation parameters are superpositions of the parameters corresponding to annihilations in a single state. For the S parameter we can write

$$S = \sum_i \eta_i S_i, \quad (2.1)$$

where η_i is the fraction of positrons annihilating at state i and S_i is the S parameter of state i . An identical equation holds for the S parameter with the same annihilation fractions. In the case of only two annihilation states whose relative intensity changes the annihilation parameters fall on a line in the S - W -plane, which can be used to identify the defects and their concentration [5]. By using the trapping rate into a defect κ_D and the positron lifetime from the delocalized bulk state τ_B , the concentration of the defects can be estimated as

$$c_D = \frac{\kappa_D N_{at}}{\mu_D} = \frac{N_{at}}{\mu_D \tau_B} \frac{(P - P_B)}{(P_D - P)}, \quad (2.2)$$

where N_{at} is the atomic density, μ_D the positron trapping coefficient and P_D , P_B and P are either the S or the W parameter in the defect state, bulk state and the measured annihilation parameter, respectively [5]. In semiconductors the temperature behavior of μ_D depends on the charge of the defect. For positive vacancies μ_D is small and thus they are usually not detected. For neutral defects the positron trapping coefficient is temperature independent with values around 10^{14} - 10^{15} s⁻¹ and for negatively charged vacancies μ_{V^-} varies as $T^{-0.5}$, and has a typical value of 2×10^{15} s⁻¹ at 400 K. The trapping rates into negative and neutral defects limit the detectable vacancy concentration to above approximately 10^{15} cm⁻³ [5].

The defect concentration can also be estimated using the positron diffusion length, as in Publication I. If the positron diffusion length in defect free material L_B is known and the diffusion length in defected material L is much shorter than L_B , then the defect concentration is given by [5]

$$c_D = \frac{(L_B/L)^2 N_{at}}{\mu_D \tau_B}. \quad (2.3)$$

The temperature dependence of the trapping coefficients affects the measured annihilation parameters. Increased trapping rate into defects leads to a higher annihilation fraction in defects and a lower fraction in the bulk state. According to Eq. 2.1 the measured annihilation parameters are superpositions of annihilations in different states. Therefore the measured S parameter in a samples with negative vacancies increases when the sample temperature is decreased due to more positrons annihilating at vacancies corresponding to a high S parameter.

Trapped positrons may escape from the trap when the positron thermal energy is high enough. For example binding energy negative ions or dislocations is low and trapping is only observed at temperatures below 200 K. Above room temperature positrons are trapped by vacancies but the signal from the shallow traps vanishes as positrons are able to escape from them. The vacancy concentration can be determined from the measurement at high temperatures. This has been used earlier to identify negatively charged ions or dislocations in GaN [9, 10]. However, in case all the positrons already annihilate at negatively charged defects at high temperatures the annihilation fractions cannot change with temperature and the annihilation parameters remain constant, as in some samples studied in this thesis.

To support the measurements the electron momentum distributions can be calculated theoretically for different vacancy-donor complexes. In this thesis the atomic superposition method was used in the calculations [7, 8, 11–13]. In addition, some data was calculated with a more accurate *ab initio* method [14]. Results using both methods agree well at momenta higher than $15 \times 10^{-3} m_0 c$, while only the

ab initio calculations produce reliable results at lower momenta corresponding to the valence electrons.

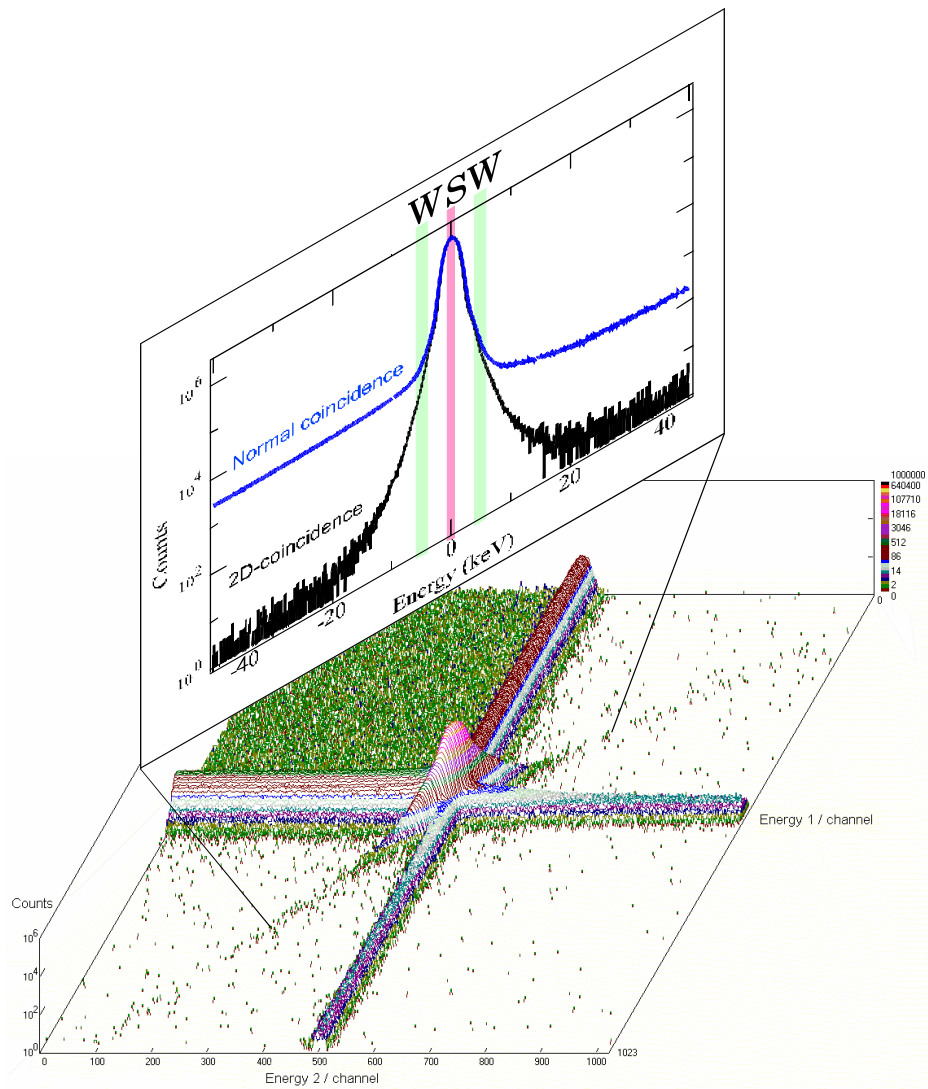


Figure 2.1: Two dimensional Doppler spectrum from a coincidence measurement. One dimensional Doppler spectrum is obtained from the figure diagonal in a 2-D coincidence measurement. In a 1-D measurement the spectrum is obtained in horizontal or vertical direction. The difference in background levels and the definition of the shape parameters S and W are shown in the inset.

Chapter 3

Defects in Silicon Related Materials

Silicon has been the dominant material in integrated circuits for decades. Increasing the conductivity of the material is required to improve the device performance. Higher conductivity of Si is achieved by increasing the charge carrier density or the mobility of the charge carriers. Doping the material with impurities to higher and higher concentrations is used to increase the carrier density. Fundamental material problems start to appear when Si is doped to concentrations above $\approx 3 \times 10^{20} \text{ cm}^{-3}$.

The electron and especially hole mobility in germanium is much higher than in Si. Also, strain increases the electron and hole mobilities [15]. Therefore, significant increase in the performance of transistors can be achieved mixing silicon with germanium and constructing strained SiGe/Si heterostructures [16, 17]. Strained silicon germanium is currently being used in high-end microprocessors by Intel. In addition, the band gap of $\text{Si}_{1-x}\text{Ge}_x$ alloys can be varied between the gaps of Si and Ge. The ability to incorporate SiGe into existing silicon based manufacturing processes is a further advantage of the material [18]. Further increase in the conductivity can be achieved by using pure Ge or Ge rich $\text{Si}_{1-x}\text{Ge}_x$ alloys. Ge based devices are not commonly available as Ge is expensive.

3.1 Highly doped silicon

The interest in highly doped Si is fundamentally related to the miniaturization of field-effect transistors, where increased doping is needed to maintain a sufficient conductance of the source and drain regions [19]. The free electron concentration in *n*-type Si, however, has been found to saturate at $<5 \times 10^{20} \text{ cm}^{-3}$ regardless of the doping concentration [20, 21]. This electrical deactivation has been attributed to the formation of point defects. The presence of vacancy-impurity complexes such as V-As₃ has been verified in melt-grown or ion-implanted material [22–24], and their formation has been explained by kinetic migration processes [25].

Growth by molecular beam epitaxy (MBE) at low temperature ($< 600 \text{ K}$) can be applied to achieve metastable doping and free electron concentrations, which become compensated only at doping densities $10 \times 20 \text{ cm}^{-3}$ [26]. At these very high doping levels the pairing of impurities may happen for purely statistical reasons [27, 28]. The scanning transmission electron microscopy studies have, indeed, observed donor pairs at concentrations expected for compensating defects [28, 29]. These donor pairs (DP) have been attributed to the configuration DP-V-I, where the Si atom neighboring the Sb dopant pair has relaxed towards the interstitial site (I) leaving a vacancy (V) behind [29]. The presence and size of the open volume in this defect has been deduced indirectly by comparing the positions of the Sb atoms to the theoretically predicted lattice relaxation [29]. On the other hand, the positron annihilation experiments of Szpala et al. suggest that open-volume defects larger than monovacancies may be present [30].

In Publication I we apply positron annihilation spectroscopy to study vacancies formed in the low-temperature MBE grown highly Sb-doped Si. The measurements have been performed both with the native surface oxide and after the oxide was removed by HF etching. Four Si(100) layers grown by MBE on Si substrates at 550 K were studied (Table 3.1) [26]. Sample No. 1 with the largest doping concentration was electrically highly compensated (fraction of free electron concentration n to dopant density [Sb] ≈ 0.06) while the three other samples were more active ($n/[Sb] > 0.7$).

The S parameter as a function of positron implantation energy E is shown in Figure 3.1. The S parameter increases with doping at the depth corresponding to the highly Sb-doped layer at $E = 0.5 \text{ keV}$. The $S(E)$ peaks in samples No. 1 and No. 2 show that the electron density is reduced and indicate high vacancy densities in the Sb-doped layer. The vacancies form open-volume clusters at least in sample No. 1, since $S/S_B = 1.08$ is much higher than expected for monovacancies [4]. The vacancy concentrations in the samples were estimated from positron diffusion lengths using Equation 2.3. The estimated concentrations are in the 10^{20} cm^{-3} range (Table 3.1), and thus are very significant for the compensation of the Sb

Table 3.1: The Sb doping concentration and the free electron concentrations of the Si samples. The vacancy concentrations were obtained from the analysis of positron annihilation results.

Sample	Thickness nm	[Sb] cm ⁻³	n cm ⁻³	[V] cm ⁻³
#1	30	3.7×10^{21}	2.3×10^{20}	8.9×10^{20}
#2	70	9.4×10^{20}	6.5×10^{20}	1.5×10^{20}
#3	50	5.9×10^{20}	4.2×10^{20}	4.7×10^{19}
#4	30	2.7×10^{19}	2.4×10^{19}	$\leq 10^{19}$

doping.

The defects formed in MBE and their stability in subsequent heat treatments were studied especially in sample No. 2, since this doping concentration was investigated most carefully also by scanning transmission electron microscopy [28, 29]. Figure 3.2 shows the measured electron momentum density in the [100] direction, shown as scaled to that of a V-P pair (along the [111] direction) and theoretical calculations presented in Publication I. The comparison to theoretical calculations shows that no single defect type is able to explain the experimental curve at all momenta (Fig. 3.2). Several important conclusions can be made, however, by comparing the relevant parts of the curves. First, the narrowing of the momentum density at $0-3 \times 10^{-3} m_0c$ indicates that divacancies are present, since Sb-decorated monovacancies lead to momentum ratios below unity. Second, the broad peak at $10-20 \times 10^{-3} m_0c$ due to Sb $4d$ electrons is much better reproduced by monovacancy complexes V-Sb and V-Sb₂ than by the decorated divacancies. The best agreement is obtained for the V-Sb pair. Third, the ratio curve for donor pair defects DP2-V-I and DP4-V-I (defined in Ref. [29]) does not agree with the experimental data at any momentum range.

Our positron annihilation measurements, supported by theoretical predictions, show the formation of vacancies and vacancy clusters in highly Sb-doped Si grown by molecular beam epitaxy. The open-volume defects are neighbored by 1-2 Sb impurities, and their concentration is large enough to be important for the electrical deactivation of the Sb doping. Annealing experiments show that vacancy defects are unstable already at 400-500 K, below the growth temperature 550 K. The defects form larger vacancy-Sb complexes, most likely by the migration of V-Sb pairs. The results demonstrate the metastable nature of Sb doping in Si grown by low-temperature MBE and explain the high electrical activation of Sb and deactivation in annealing by migration processes of vacancy defects.

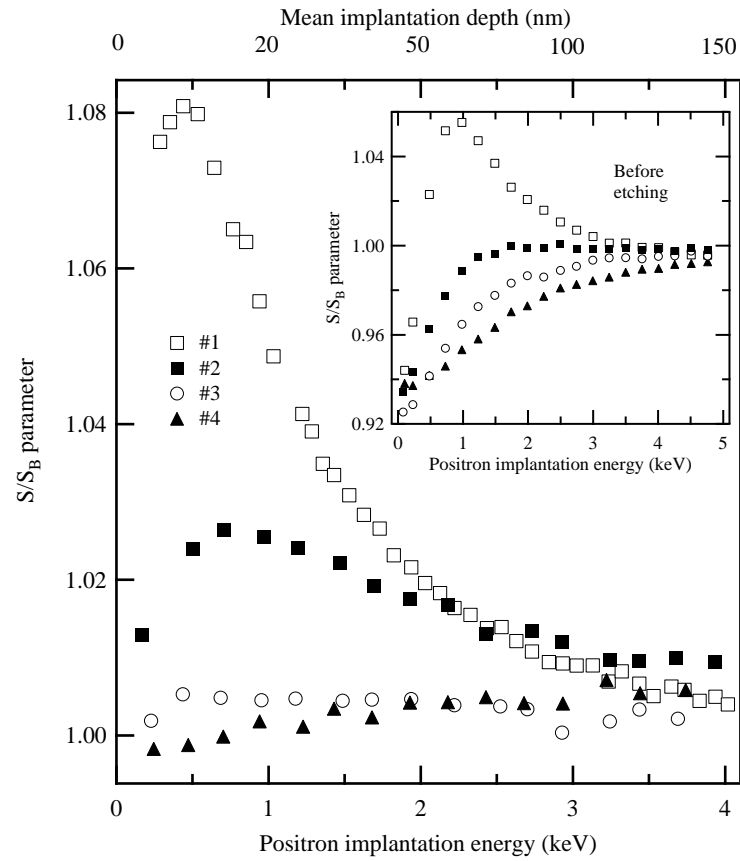


Figure 3.1: The S parameter versus the positron implantation energy in samples presented in Table 3.1. The S parameter is scaled to the bulk lattice value S_B obtained in the substrate. The inset shows the results measured in samples with the native oxide on the surface. The statistical error is smaller than the marker size in the figure.

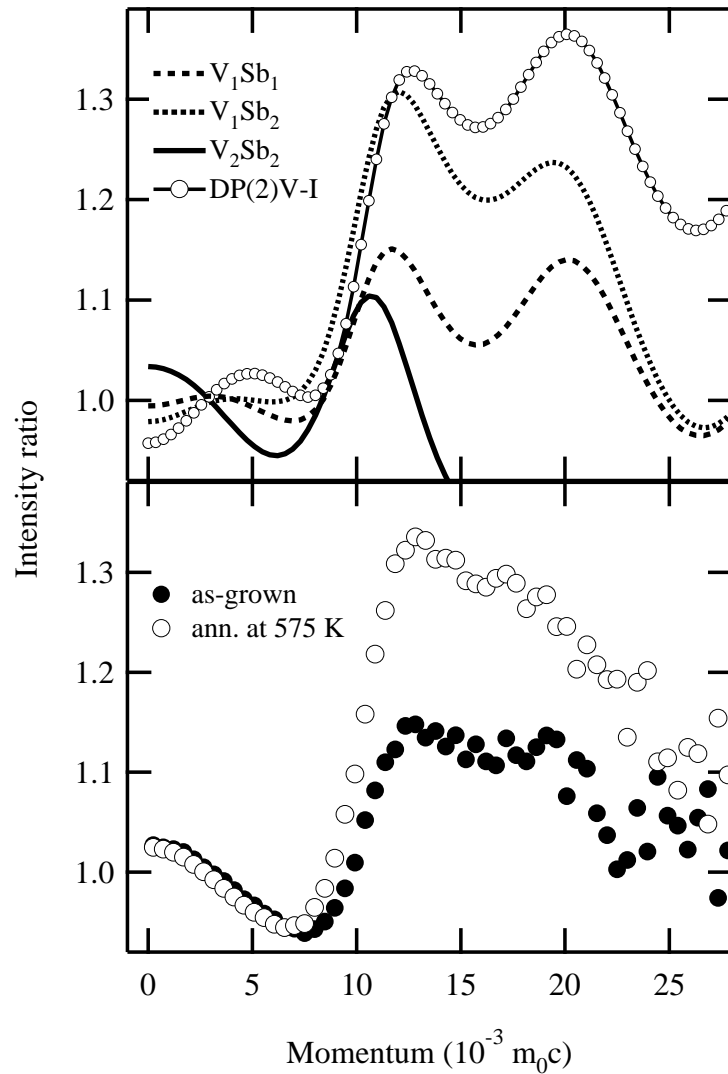


Figure 3.2: Momentum density of the vacancy defect in the as-grown Sb-doped Si (sample No. 2) and after annealing at 575 K. The measured momentum density along the [100] direction is scaled to that of the V-P pair along the [111] axis, leading to oscillations. The lines in the upper panel are obtained from theoretical calculations in various model structures. The fluctuations of nearby points show the statistical error, which grows with momentum.

3.2 Silicon germanium

Silicon germanium (SiGe) has attracted much attention for its potential use in semiconductor industry. Strained Si/SiGe heterostructures are used to enhance the electron and hole mobilities [15]. Both experimental and theoretical studies of energetics of vacancy formation in $\text{Si}_{1-x}\text{Ge}_x$ materials have shown a net energy gain of around 0.2 eV when a Ge atom replaces a Si atom next to a vacancy [31, 32]. This suggests that there could be vacancy complexes surrounded by many more Ge atoms than predicted by the atomic abundances in the material.

In Publication II we have studied relaxed phosphorus doped n -type and undoped $\text{Si}_{1-x}\text{Ge}_x$ samples with x up to 0.30. In order to study native point defects in the $\text{Si}_{1-x}\text{Ge}_x$ layers, the layers were irradiated using 2 MeV protons. The details of the studied samples are shown in Table 3.2. Proton irradiation is expected to generate a high concentration of Frenkel pairs. Both in Si and in Ge monovacancies have been shown to be mobile at room temperature [33, 34]. After irradiation only vacancies that encounter impurity atoms or other vacancies during migration remain in the samples.

Table 3.2: Properties of the studied $\text{Si}_{1-x}\text{Ge}_x$ samples.

	[Ge] (%)	Sample type	Doping [P] (cm^{-3})	Irradiation p^+ (cm^{-2})
#1	10	-	-	-
#2	10	n -type	10^{18}	-
#3	20	-	-	-
#4	20	n -type	10^{18}	-
#5	20	n -type	10^{19}	-
#6	30	-	-	-
#7	30	n -type	10^{18}	-
#8	10	n -type	10^{18}	1.6×10^{15}
#9	20	n -type	10^{18}	1.6×10^{15}
#10	30	n -type	10^{18}	1.6×10^{15}
#11	20	-	-	1.6×10^{15}

Figure 3.3 shows the SiGe layer-specific S and W parameters from the studied SiGe samples at positron implantation energy minimizing the effects of the surface and the substrate. All the as-grown samples are in an increasing order of the Ge concentration and fit well on a line joining Si and Ge, except the undoped $\text{Si}_{0.70}\text{Ge}_{0.30}$ sample. This shows that the annihilation parameters of SiGe layers

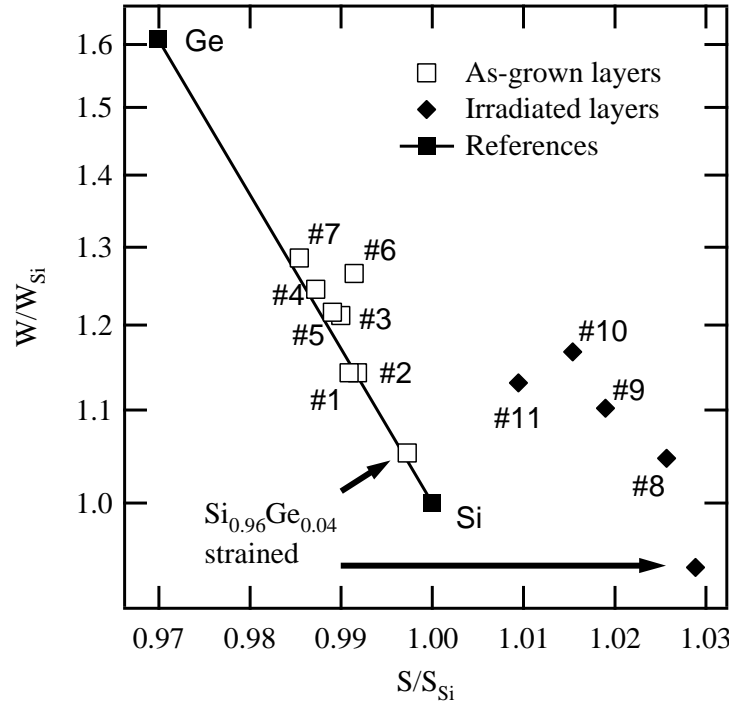


Figure 3.3: The $S - W$ parameters of all the studied SiGe layers and Ge relative to parameters of defect-free Si. All as-grown samples, except sample #6, fall on a line joining Si and Ge. Irradiated samples have a higher S and a lower W parameter indicating vacancies. The statistical error is smaller than the marker.

can be explained as superpositions of annihilations in Si and Ge lattices. Interestingly, the change of the annihilation parameters with Ge concentration seems to be larger than the Ge concentration of the lattice. The 30 % SiGe alloy leads to about 50 % effect in the S and W parameters (Fig. 3.3), showing that annihilating positrons prefer Ge atoms. All P-doped layers lie on a line between pure Si and pure Ge, which suggests that there are no positron trapping defects such as vacancies in the measured layers.

The irradiated samples have a much higher S and a lower W parameter than the corresponding as-grown samples. To identify the defects in different irradiated layers we calculated the changes in the S and W parameters relative to their corresponding $\text{Si}_{1-x}\text{Ge}_x$ bulk values, as shown in Fig. 3.4. In all P-doped layers the changes in the S and W parameters are almost equal. This shows that the defects are the same in all the samples and the changes observed relative to Si are due to the changes in the Ge concentration of the alloy. Supported by temperature dependent and co-incidence measurements we identify the dominant defect as the

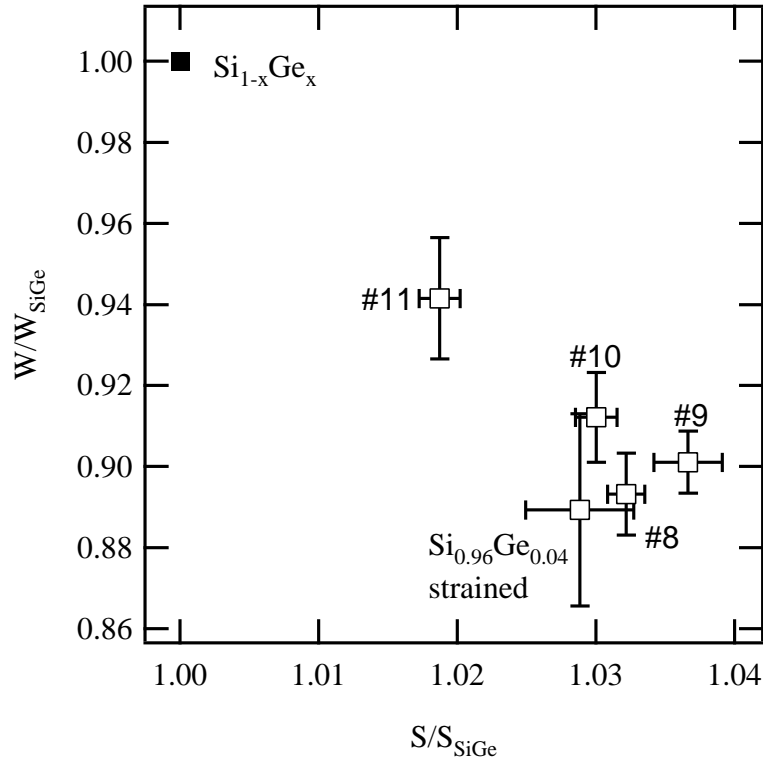


Figure 3.4: The S and W parameters in the irradiated samples relative to the as-grown ones are similar in all the n -type samples, in agreement with results that the irradiation induced defects have a similar structure.

vacancy phosphorus pair in all the P-doped layers. During migration negatively charged vacancies will experience a long range Coulomb attraction to the positive phosphorus atoms, while the potential due to lattice relaxation is very short range. Vacancies formed in the irradiation process are therefore likely to get trapped to the nearest P-atoms and the distribution of Ge atoms around the E-center then reflects the Ge concentration of the host lattice.

The irradiated undoped $Si_{0.80}Ge_{0.20}$ #11 is separate from all other layers. In the S - W plot it is located half way between the as-grown and the P-doped irradiated layers. Calculations suggest that the most abundant defect could be a monovacancy surrounded by four Ge atoms, whose formation energy is approximately 1 eV lower than that of $V-Si_4$ [32]. In contrast to the theoretical prediction the measured S and W parameters cannot be from defect complexes with many Ge atoms. Rather we show that the undoped layers contain a low concentration of divacancies or larger defects.

3.3 Germanium

The world's first transistor was made of germanium. It was invented in 1947 by Shockley, Bardeen and Brattain. Germanium was soon replaced by silicon in producing efficient semiconductor transistors. Recently Ge has re-emerged as a material of choice for high-performance devices because of the higher electron and hole mobilities despite being more expensive and harder to process than Si. Germanium crystals easily turn amorphous under ion implantation, which is required in many processing stages. Understanding the defects created in the implantation is needed to understand the amorphization and recrystallization by a subsequent heat treatment.

In Publication III we have studied defects in Si and Ge implanted Ge and the annealing of the defects. Positron annihilation spectroscopy has been combined with Rutherford backscattering/channeling (RBS/C) and deep level transient spectroscopy. The implantation fluences of the samples ranged from $1 \times 10^{12} \text{ cm}^{-2}$ to $4 \times 10^{14} \text{ cm}^{-2}$ and the implantation depth of the ions was approximately $1 \mu\text{m}$. RBS/C revealed that amorphization occurred in the samples implanted with the highest fluences and already a Ge fluence as low as $1 \times 10^{13} \text{ cm}^{-2}$ results in 65-75 % of the atoms being displaced.

The ion implantation damage in the samples was studied by measuring the PAS spectra as a function of the positron implantation energy. The measured S and W parameters are similar in all the as-implanted samples (see Fig. 3.1 of Publication III). The $S(E)$ curve is flat for all but the sample with the lowest implantation fluence. The measured S parameter is 4.7 % over the level observed in bulk Ge, which would be expected for defects with an open volume approximately of a divacancy. Similar annihilation parameters show that the same type of defects is present and the concentration of positron trapping defects is high enough to produce saturated trapping into open volume defects. Similar saturation of the annihilation parameters after ion implantation has been found earlier in Si [35].

The implanted layers were annealed at 200 - 500 °C for 30 min to study the temperature evolution of the defects created. The measured curves for the S parameter in the sample with the Si fluence $1 \times 10^{12} \text{ cm}^{-2}$ for different annealing temperatures are shown in Fig. 3.5. At low positron implantation energies we observe the sample surface and the unimplanted wafer at $E > 20 \text{ keV}$. After annealing a peak in the S parameter forms between energies 5 - 20 keV that corresponds to defects in the implanted layer. After annealing at 200 °C the S parameter peaks at $S=1.09$. The S parameter is closely related to the open volume of the defects and the observations suggest that the vacancies observed after 200 °C anneal have more than twice the open volume of the defects in the as-implanted sample. Annealing the samples at temperatures 300, 400 and

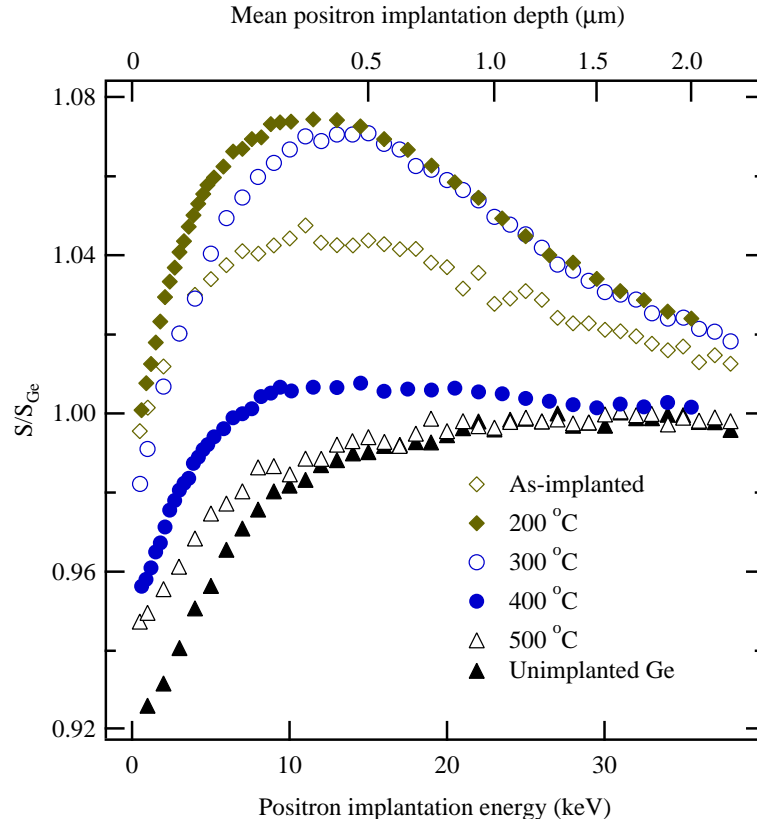


Figure 3.5: The low momentum S parameter measured at room temperature after 30 min anneal for samples implanted with Si fluence $1 \times 10^{12} \text{ cm}^{-2}$. The data has been scaled to the parameters measured in bulk Ge with $S_{Ge} = 0.517$.

500 °C the S parameter decreases approximately to the level observed in the bulk Ge. This shows that most defects anneal out of the sample by 500 °C. The annealing temperature of the observed vacancy clusters is similar to what Krause-Rehberg *et al.* [36] found in high-stress and low-temperature deformed high purity germanium.

Figure 3.6 shows the annealing behavior of the highest implantation fluence for the Si implanted samples. The behavior is quite different from the lower fluencies. At 200 °C a peak in the S parameter starts to develop at a depth of approximately 1 μm . When the annealing temperature is increased to 300 °C a second peak near the surface appears in the sample. The near surface peak continues to grow and reaches approximately the same S parameter value as the single peak observed in the samples implanted with a lower fluence. The peak at 1 μm grows

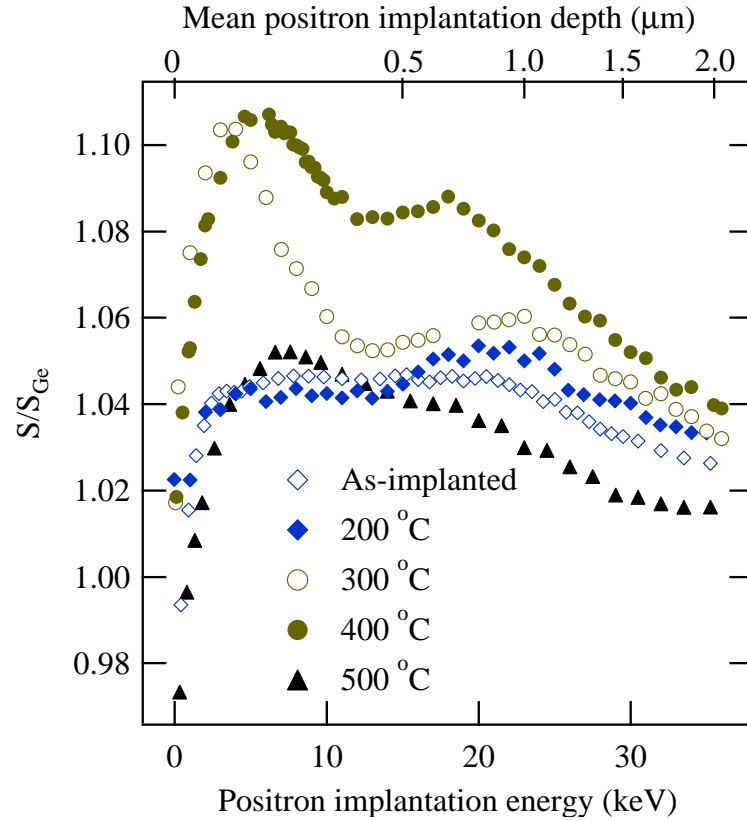


Figure 3.6: The low momentum S parameter measured at room temperature after 30 min anneal for the samples implanted with Si fluence $4 \times 10^{14} \text{ cm}^{-2}$. The data has been scaled to the parameters measured in bulk Ge with $S_{Ge}=0.517$.

with increasing annealing temperature and a slight shift towards the surface can also be seen. Even after annealing at 500 °C, although some defect recovery is observed, the annihilation parameters are clearly different from defect free Ge. This could be due to the zipper band observed in RBS/C study, which could prohibit or slow down the agglomeration of vacancy defects into larger clusters.

Chapter 4

Defects in Gallium Nitride

Gallium nitride is used in light emitting diodes (LEDs) to produce blue light and in high power electronics [2]. The material is naturally *n*-type due to residual impurities and therefore doping it *p*-type is difficult. Bulk GaN is expensive as growth of single crystals is done at high pressure and at high temperature [37, 38]. Therefore components are typically made of epilayers grown on foreign substrates such as sapphire or silicon carbide (SiC). The lattice constant mismatch and the different thermal expansion coefficient induce stress in the GaN layer, which relaxes through the formation of dislocations. The dislocation densities often reach the 10^{10} cm^{-2} range [2, 39]. Using misoriented substrates some of the stress could be relieved, enabling the production of GaN material with a lower defect density.

Usually the GaN crystal structure is wurtzite but it also exists in cubic form. In the wurtzite structure the growth can take place in several directions. The growth characteristics, such as the growth speed and the impurity incorporation, depend on the growth direction. Growth in the *c*-direction can take place in both Ga-polar and N-polar modes corresponding to different stacking orders of Ga and N atoms. Growth in the Ga-polar (0001) direction generally leads to a smooth surface morphology and a high quality material, while N-polar (000 $\bar{1}$) growth is much more difficult. N-polar growth may be desirable since it is more easily etched [40, 41]. In N-polar GaN the surface reactivity is increased enhancing oxygen incorporation by one to two orders of magnitude [42, 43].

4.1 SiC as substrate material

Silicon carbide is a promising substrate material for GaN growth. SiC has a relatively small lattice mismatch and a high thermal conductivity, which makes it suitable for high power applications [44]. By using misoriented SiC substrates in molecular beam epitaxy the threading screw dislocation density can be reduced by two orders of magnitude and the edge dislocation density by one order of magnitude. On misoriented substrates the growth mode changes to the two dimensional step-flow mode [45, 46]. However, cracks are observed to form in layers grown on misoriented substrates using metal-organic chemical vapour deposition (MOCVD) [47].

In Publication IV we report on defects observed in GaN epilayers grown on misoriented 4H-SiC substrates. The studied samples were grown by MOCVD at 1170 °C, as described in Ref. [47]. In the three samples studied the substrate was tilted by 0°, 3.4° and 8° from $\langle 0001 \rangle$ towards $\langle 11\bar{2}0 \rangle$. The samples with a tilted substrate had cracks with an average separation of 50 μm and 15 μm for the misorientation angles 3.4° and 8°, respectively.

The S parameter curves were measured in the samples at room temperature as a function of the positron implantation energy. In all the samples the S parameter is higher and the W parameter lower than in the bulk GaN lattice indicating the presence of vacancies. The S parameter is highest in the 8° off-axis sample, second highest in the 3.4° off-axis sample and lowest in the on-axis sample (see Fig. 1 of Publication IV).

The temperature dependence of positron trapping into defects was used to identify the defects and estimate their concentration. In undoped GaN vacancies have been shown to be in their negative charge state [48], which affects the temperature behavior of the parameters. Figure 4.1 shows the S parameter as a function of the measurement temperature for all the samples. The misoriented samples have a constant S parameter at temperatures below 100 K. The S value increases with temperature in the range 150–400 K, and above 400 K it becomes constant again. This kind of behavior is typical when shallow traps and vacancies co-exist in the sample competing as positron traps [5]. The S parameter in the on-axis sample is constant at low temperatures up to 250 K, which suggests that we observe saturated trapping into shallow traps at these temperatures. This indicates that the S value measured at low temperatures in the on-axis sample is slightly higher than that of the bulk GaN and specific to the shallow trap.

To identify the defects, the measured W parameters of the temperature dependent measurements plotted as a function of the S parameter and compared with the annihilation parameters of Ga vacancies and vacancy clusters, which have been

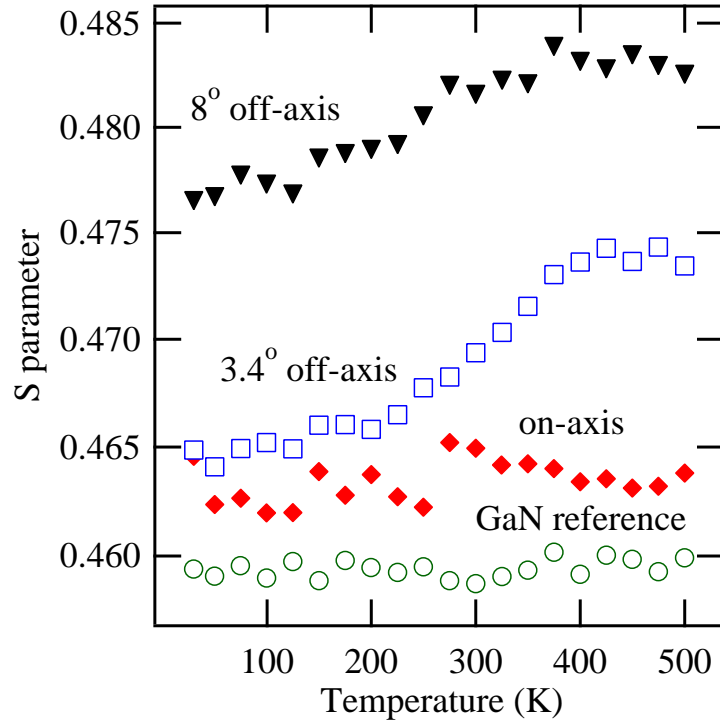


Figure 4.1: The S parameter as a function of measurement temperature at 15 keV positron implantation energy in GaN grown on misoriented SiC.

determined earlier [48–50]. All the measured parameters fall on a line that lies between those joining the bulk GaN to the V_{Ga} and the bulk GaN to the V_{clust} . The annihilation parameters are superpositions of the parameters corresponding to positrons annihilating from different states. We can estimate the relative concentrations of the defects from the slope of the line in the (S, W) plane: about 50 % of the observed defects are Ga vacancies and 50 % are larger vacancy clusters.

The concentration of vacancy type defects can be estimated from the measurement points above 400 K (where only vacancies act as positron traps). The defect specific S parameter S_V can be extrapolated from the point where the line fitted to the measurement data intersects the line between the points of V_{Ga} and V_{clust} . The estimated vacancy concentrations vary from $4 \times 10^{16} \text{ cm}^{-3}$ in the on-axis sample to $7 \times 10^{17} \text{ cm}^{-3}$ in the 8° off-axis sample. Both vacancy concentration and free electron concentration increase with increasing angle of misorientation [47], as expected for negative vacancies. The trapping rate to shallow traps κ_{ST} can be estimated from the low temperature data where no detrapping from the shallow traps occurs [5]. The data shows that the trapping rate to the shallow

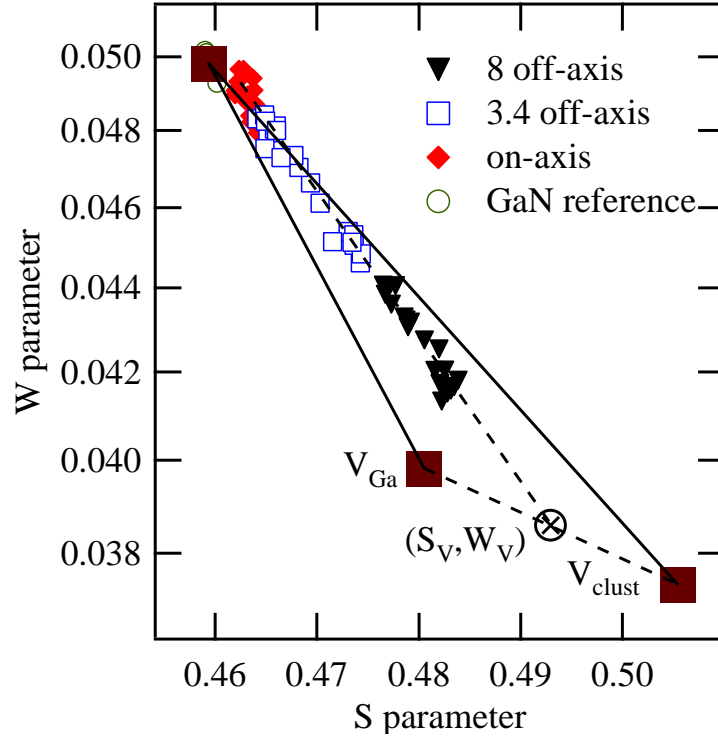


Figure 4.2: The (S, W) parameters measured as a function of temperature in the GaN samples. The (S, W) values corresponding to the vacancy free GaN (S_B, W_B), the Ga vacancy ($S_{V,Ga}, W_{V,Ga}$), and a vacancy cluster (S_{clust}, W_{clust}) are shown [48–50]. The dotted lines show the fitting procedure used to determine the relative concentrations of the Ga vacancies and the vacancy clusters, as well as the parameter S_V used to estimate the absolute defect concentrations.

traps decreases from over $2 \times 10^{11} \text{ s}^{-1}$ in the on-axis sample to $5 \times 10^{10} \text{ s}^{-1}$ in the 8° off-axis sample.

The observed shallow positron traps are likely to be dislocations. They contain a small open volume whereas the S parameter corresponding to negative ions is the same as in the GaN lattice [10] and are not associated with the cracks described by M. Rudzinski *et al.* [47]. As the trapping rates are proportional to the defect densities, we can conclude that the dislocation density is higher in layers with the less misoriented substrate. This result is in good agreement with the results obtained by defect-selective etching experiments [47].

4.2 Growth polarity

The properties of gallium nitride depend strongly on the crystal orientation and the polarity of the growth direction. Growth in the Ga-polar (0001) direction generally leads to a smooth surface morphology and high quality material, while N-polar (000 $\bar{1}$) growth is much more difficult [40, 41]. The stoichiometry of Ga and N overpressures during the growth is also important [40]. Generally molecular beam epitaxy of GaN takes place in gallium stable conditions, where the diffusivity of gallium adatoms is high at the surface [40, 51]. Approaching nitrogen stable growth, however, the surface mobility of Ga adatoms is reduced due to Ga-N bonds [40, 51] and the surface reactivity is increased enhancing oxygen incorporation by orders of magnitude [42, 43].

Experimental and theoretical studies demonstrate the influence of growth polarity and stoichiometry on the impurity incorporation [42, 43, 52]. Epitaxial N-polar GaN contains typically an order-of-magnitude more oxygen than Ga-polar layers, and when approaching N-stable conditions the oxygen incorporation is strongly enhanced for both polarities [42].

In Publication V we apply positron annihilation spectroscopy to study the formation of vacancy defects in GaN grown in different polar orientations and under different stoichiometry conditions. The O-doped GaN layers (Table 4.1) were grown at West Virginia University (WVU) by rf plasma-assisted MBE, as described in Refs. [42, 53]. The N-polarity GaN was grown by nucleating GaN buffer layers directly on sapphire in highly Ga-rich conditions. The Ga-polarity GaN was prepared by epitaxy on (0001) GaN templates grown by MOCVD on A-plane sapphire at the Naval Research Laboratory. The stoichiometry was varied by changing the beam-equivalent pressure (BEP) of Ga, as shown in Table 4.1.

The samples show two kinds of behavior. The GaN layer specific parameters could be clearly identified in all the N-polar samples (#1 to #5) and the Ga-polar samples #6 to #9. In the other Ga-polar samples, #10 to #15 the annihilation parameters change continuously from the surface to the parameters of the substrate and the layer specific parameters cannot be estimated reliably. The defects were identified using the S - W plot shown in Fig. 4.3. The points corresponding to the GaN layers form two separate groups. In the N-polar samples #1 to #4 the parameters characterizing the MBE layer are approximately the same. In the N-polar sample #5 the S parameter is clearly lower and the W parameter higher, possibly reflecting the heavy O-doping. The Ga-polar samples #6 to #9 have similar annihilation characteristics as the N-polar sample #5.

In Fig. 4.3 the (S, W) values from the Ga-polar samples #6 to #9 and the N-polar sample #5 fall very close to the point characteristic of the Ga vacancy, suggesting a high V_{Ga} concentration. On the other hand, the slope of the line between the

Table 4.1: The polarity, thickness, beam equivalent pressure of Ga, O-partial pressure p_{O_2} , dopant concentration [O] and the conduction electron concentration [n] in the studied MBE-grown GaN layers.

Polarity and Thickness (μm)			BEP (Ga) (10^{-6} torr)	p_{O_2} (torr)	[O] (cm^{-3})	n (cm^{-3})
#1	N	1	1.6	4.0×10^{-12}		1.0×10^{15}
#2	N	1	0.96	5.0×10^{-10}		1.7×10^{18}
#3	N	1	1.4	4.0×10^{-11}	3.0×10^{16}	6.0×10^{16}
#4	N	1	1.6	4.0×10^{-11}	3.0×10^{16}	6.6×10^{16}
#5	N	1	0.5	1.0×10^{-7}		6.8×10^{19}
#6	Ga	1.8	0.49	1.5×10^{-7}	2.5×10^{22}	3.0×10^{20}
#7	Ga	1.8	0.46	5.5×10^{-8}		9.0×10^{19}
#8	Ga	1	0.48	5.0×10^{-8}	2.6×10^{21}	4.0×10^{17}
#9	Ga	1.36	0.49	2.0×10^{-7}	1.5×10^{22}	7.4×10^{19}
#10	Ga	0.62	0.95	1.1×10^{-7}	1.5×10^{18}	1.4×10^{18}
#11	Ga	1.9	1.2	4.0×10^{-12}	$< 1 \times 10^{16}$	3.8×10^{17}
#12	Ga	0.9	0.93	1.0×10^{-9}	5.0×10^{16}	2.8×10^{16}
#13	Ga	1	1.6	3.0×10^{-11}		3.0×10^{17}
#14	Ga	1	0.73	2.0×10^{-10}	1.0×10^{16}	1.2×10^{16}
#15	Ga	1	1	2.0×10^{-8}	3.0×10^{17}	3.0×10^{17}

(S, W) points of the N-polar samples #1–4 and the vacancy-free lattice (S_b, W_b) coincides very well with that characteristic to the previously observed vacancy cluster. The positron trapping at the vacancy clusters is also evidenced by the very high S parameter, $S/S_b \approx 1.08$, which is much higher than typically observed for monovacancies [5].

Interestingly, the Ga vacancies are detected in high concentrations only in the samples where the gallium BEP is low, $\sim 0.5 \times 10^{-6}$ torr, which means the growth approaches nitrogen stable conditions [42]. A high V_{Ga} concentration is found both in Ga-polar samples and the N-polar sample with a low Ga BEP (see Fig 4.3). Due to the saturation trapping into vacancies it is only possible to give a lower limit estimate, $[V_{Ga}] \gtrsim 5 \times 10^{18} \text{cm}^{-3}$ [5]. Also, the incorporation of oxygen is significantly increased both in Ga-polar and N-polar growth direction when the growth is N-stable [42]. The observed high V_{Ga} concentration in the N-stable samples agrees with the theoretical calculations, predicting the formation of compensating V_{Ga} should be enhanced in the strongly n -type material [54, 55].

The positron annihilation experiments in irradiated GaN have shown that the isolated V_{Ga} are mobile and recover by migration already at 300 °C [56]. Thus

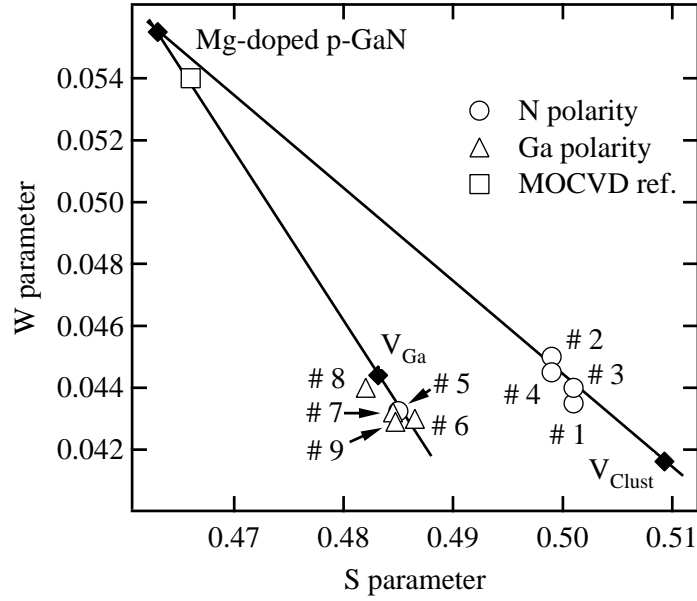


Figure 4.3: The S - W plot of (S, W) values characterizing the MBE-layers. The (S, W) values corresponding to vacancy free Mg-doped GaN (S_b, W_b), Ga vacancy ($S_{V_{Ga}}, W_{V_{Ga}}$), and vacancy cluster (S_{clust}, W_{clust}) are also shown. The statistical error is smaller than the marker size.

the observed vacancies are most probably V_{Ga} -donor-impurity pairs ($V_{Ga}-O_N$ in this case), which can survive the cooling down from the growth temperature. The presence of the Ga vacancies only in the samples with the high oxygen content (N-stable growth) thus agrees also with idea of the essential role of oxygen both in decreasing the formation energy of Ga vacancies and enhancing their stability [57].

In Ga-polar layers grown in Ga-stable conditions (samples #10–15) we do not observe high vacancy concentrations. This is in good agreement with the electrical properties which show very little compensation [42]. Controlled oxygen doping can thus be done up to the level of 10^{18} cm^{-3} without significant formation of compensating Ga vacancies.

The observation of the vacancy clusters in the N-polar layers grown in Ga-stable conditions is very interesting. The SIMS and Hall data of these and other samples [53] show that they are relatively uncompensated, suggesting the observed vacancies should be electrically neutral. Positron trapping at similar vacancy clusters has been observed earlier in MBE GaN layers [49, 50, 58]. It seems that the formation of clusters is related to the N-polar growth direction of the layer.

When the oxygen doping level is low the Ga-polar layers show no significant vacancy concentrations, while in the N-polar layers high concentrations of vacancy clusters are formed. The higher reactivity of the $(000\bar{1})$ surface enhances the incorporation of oxygen impurities [42], but according to this work also enables the formation of vacancy clusters. This may be one of the limiting factors for N-polar MBE-growth of GaN.

Chapter 5

Summary

In this thesis the properties of point defects in gallium nitride and silicon related materials were studied by positron annihilation spectroscopy. Doppler broadening measurements of the 511 keV annihilation line were used to characterize defects on the atomic level. In publications I we observe vacancy dopant atom pairs in highly Sb-doped Si at concentrations relevant to the observed electrical compensation. It is possible to grow silicon with an extremely high charge carrier density at low temperatures. However, metastable vacancies and vacancy clusters are formed. In Publication II we find that vacancy donor pairs are formed in proton irradiated $\text{Si}_{1-x}\text{Ge}_x$ and the surroundings of the defects are independent of the Ge concentration of the underlying lattice. Also, no vacancy defects with several Ge atoms surrounding it were found.

In Publication III we used silicon and germanium ion implantation to generate defects in *n*-type Ge. The annihilation parameters recorded in all the as-implanted samples were similar even though Rutherford backscattering measurements show that at the highest implantation fluences the material amorphizes. On average the defects have approximately the size of a divacancy. In subsequent heat treatments the defects form vacancy clusters with at least twice the size of defects in the as-implanted samples. When the annealing temperature is increased further the vacancy type defects are found to recover. The size of the clusters observed and the temperature needed to remove the defects increases with ion fluence.

In Publications IV and V we study the properties of GaN epilayers and the effect of growth direction on the defects formed. In GaN grown on misoriented 4H-SiC substrates we observe simple vacancies and vacancy clusters for all substrate orientations. Also, we observe shallow positron traps identified as dislocations. The vacancy concentration increases and the concentration of dislocations decreases with the increasing substrate misorientation. Defects in molecular beam epitaxy

grown O-doped GaN depend strongly on the growth stoichiometry and doping density. Ga-polar GaN is free of compensating Ga vacancies up to $[O]=10^{18}$ cm^{-3} in Ga stable growth, but high concentrations of vacancies are formed in N-stable conditions. Also, vacancy clusters are formed in N-polar material grown in Ga stable conditions, which may be related to the higher reactivity of the N-polar surface.

Bibliography

- [1] M. L. Lee, E. A. Fitzgerald, M. T. Bulsara, M. T. Currie, and A. Lochtefeld, *J. Appl. Phys.* **97**, 011101 (2005).
- [2] D. J. Smith, D. Chandrasekhar, B. Sverdlov, A. Botchkarev, A. Salvador, and H. Morkoc, *Appl. Phys. Lett.* **67**, 1830 (1995).
- [3] P. M. Fahey, P. B. Griffin, and J. D. Plummer, *Rev. Mod. Phys.* **61**, 289 (1989).
- [4] R. Krause-Rehberg and H. S. Leipner, *Positron Annihilation in Semiconductors* (Springer, Berlin, 1999).
- [5] K. Saarinen, P. Hautojärvi, and C. Corbel, in *Identification of Defects in Semiconductors*, edited by M. Stavola (Academic Press, New York, 1998), p. 209.
- [6] M. Puska and R. M. Nieminen, *Rev. Mod. Phys.* **66**, 841 (1994).
- [7] M. Alatalo, H. Kauppinen, K. Saarinen, M. J. Puska, J. Mäkinen, P. Hautojärvi, and R. M. Nieminen, *Phys. Rev. B* **51**, 4176 (1995).
- [8] M. Alatalo, B. Barbiellini, M. Hakala, H. Kauppinen, T. Korhonen, M. J. Puska, K. Saarinen, P. Hautojärvi, and R. M. Nieminen, *Phys. Rev. B* **54**, 2397 (1996).
- [9] K. Saarinen, J. Nissilä, P. Hautojärvi, J. Likonen, T. Suski, I. Grzegory, B. Lucznik, and S. Porowski, *Appl. Phys. Lett.* **75**, 2441 (1999).
- [10] J. Oila, K. Saarinen, A. E. Wickenden, D. D. Koleske, R. L. Henry, and M. E. Twigg, *Appl. Phys. Lett.* **82**, 1021 (2003).
- [11] B. Barbiellini, M. J. Puska, T. Torsti, and R. Nieminen, *Phys. Rev. B* **51**, 7341 (1995).
- [12] B. Barbiellini, M. J. Puska, T. Korhonen, A. Harju, T. Torsti, and R. Nieminen, *Phys. Rev. B* **53**, 16201 (1996).

- [13] M. J. Puska and R. M. Nieminen, *J. Phys. F: Met. Phys.* **13**, 333 (1983).
- [14] M. Hakala, M. J. Puska, and R. M. Nieminen, *Phys. Rev. B* **57**, 7621 (1998).
- [15] F. Schäffler, *Semicond. Sci. Technol.* **12**, 1515 (1997).
- [16] S. Verdonckt-Vandebroek, E. F. Crabbe, B. S. Meyerson, D. L. Harame, P. J. Restle, J. M. C. Stork, and J. B. Johnson, *IEEE Trans. Electron Devices* **41**, 90 (1994).
- [17] S. E. Thompson, M. Armstrong, C. Auth, S. Cea, R. Chau, G. Glass, T. Hoffman, J. Klaus, M. Zhiyong, B. McIntyre, A. Murthy, B. Obradovic, L. Shifren, S. Sivakumar, S. Tyagi, T. Ghani, K. Mistry, M. Bohr, and Y. El-Mansy, *IEEE Electron Device Lett.* **25**, 191 (2004).
- [18] J. J. Browne, *Microwaves RF* **38**, 121 (1999).
- [19] P. A. Packan, *Science* **285**, 2079 (1999).
- [20] P. M. Fahey, P. B. Griffin, and J. D. Plummer, *Rev. Mod. Phys.* **61**, 289 (1989).
- [21] A. Lietoila, J. F. Gibbons, and T. W. Sigmon, *Appl. Phys. Lett.* **36**, 765 (1980).
- [22] D. W. Lawther, U. Myler, P. J. Simpson, P. M. Rousseau, P. B. Griffin, and J. D. Plummer, *Appl. Phys. Lett.* **67**, 3575 (1995).
- [23] K. Saarinen, J. Nissilä, H. Kauppinen, M. Hakala, M. J. Puska, P. Hautojärvi, and C. Corbel, *Phys. Rev. Lett.* **82**, 1883 (1999).
- [24] V. Ranki, K. Saarinen, J. Fage-Pedersen, J. Lundsgaard Hansen, and A. Nylandsted Larsen, *Phys. Rev. B* **67**, 041201 (2003).
- [25] V. Ranki, J. Nissilä, and K. Saarinen, *Phys. Rev. Lett.* **88**, 105506 (2002).
- [26] H.-J. Gossmann, F. C. Unterwald, and H. S. Luftman, *J. Appl. Phys.* **73**, 8237 (1993).
- [27] D. J. Chadi, P. H. Citrin, C. H. Park, D. L. Adler, M. A. Marcus, and H.-J. Gossmann, *Phys. Rev. Lett.* **79**, 4834 (1997).
- [28] P. M. Voyles, D. A. Muller, J. L. Grazul, P. H. Citrin, and H.-J. Gossmann, *Nature* **416**, 826 (2002).
- [29] P. M. Voyles, D. J. Chadi, P. H. Citrin, D. A. Muller, J. L. Grazul, P. A. Northrup, and H.-J. L. Gossmann, *Phys. Rev. Lett.* **91**, 125505 (2003).

- [30] S. Szpala, P. Asoka-Kumar, B. Nielsen, J. P. Peng, S. Hayakawa, and K. G. Lynn, *Phys. Rev. B* **54**, 4722 (1996).
- [31] S.-L. Sihto, J. Slotte, J. Lento, K. Saarinen, E. V. Monakhov, A. Y. Kuznetsov, and B. G. Svensson, *Phys. Rev. B* **68**, 115307 (2003).
- [32] P. Boguslawski and J. Bernholc, *Phys. Rev. B* **59**, 1567 (1999).
- [33] G. D. Watkins, in *Deep Centers in Semiconductors*, edited by S. T. Pantelides (Gordon and Breach Science, New York, 1986), p. 209.
- [34] P. Ehrhart and H. Zillgen, *J. Appl. Phys.* **85**, 3503 (1999).
- [35] B. Nielsen, O. W. Holland, T. C. Leung, and K. G. Lynn, *J. Appl. Phys.* **74**, 1636 (1993).
- [36] R. Kause-Rehberg, M. Brohl, H. S. Leipner, T. Drost, A. Polity, U. Beyer, and H. Alexander, *Phys. Rev. B* **47**, 13266 (1993).
- [37] J. Karpinski, J. Jun, and S. Porowski, *J. Crystal Growth* **66**, 1 (1984).
- [38] M. Leszczynski, I. Grzegory, H. Teisseyre, T. Suski, M. Bockowski, J. Jun, J. M. Baranowski, S. Porowski, and J. Domagala, *J. Crystal Growth* **169**, 235 (1996).
- [39] X. H. Wu, L. M. Brown, D. Kapolnek, S. Keller, S. P. DenBaars, and J. S. Speck, *J. Appl. Phys.* **80**, 3228 (1996).
- [40] E. J. Tarsa, B. Heying, X. H. Wu, S. P. DenBaars, and J. S. Speck, *J. Appl. Phys.* **82**, 5472 (1997).
- [41] M. Seelmann-Eggebert, J. L. Weyher, H. Obloh, H. Zimmermann, A. Rar, and S. Porowski, *Appl. Phys. Lett.* **71**, 2635 (1997).
- [42] A. J. Ptak, L. J. Holbert, L. Ting, C. H. Swartz, M. Moldovan, N. C. Giles, T. H. Myers, P. V. Lierde, C. Tian, R. A. Hockett, S. Mitha, A. E. Wickenden, D. D. Koleske, and R. L. Henry, *Appl. Phys. Lett.* **79**, 2740 (2001).
- [43] T. Zywietz, J. Neugebauer, and M. Scheffler, *Appl. Phys. Lett.* **74**, 1695 (1999).
- [44] H. Morkoç, S. Strite, G. B. Gao, M. E. Lin, B. Sverdlov, and M. Burns, *J. Appl. Phys.* **76**, 1363 (1994).
- [45] M. H. Xie, L. X. Zheng, S. H. Cheung, Y. F. Ng, H. Wu, S. Y. Tong, and N. Ohtani, *Appl. Phys. Lett.* **77**, 1105 (2000).

- [46] M. H. Xie, S. M. Seutter, W. K. Zhu, L. X. Zheng, H. Wu, and S. Y. Tong, *Phys. Rev. Lett.* **82**, 2749 (1999).
- [47] M. Rudzinski, P. R. Hageman, A. P. Grzegorzczuk, L. Macht, T. C. Rödle, H. F. F. Jos, and P. K. Larsen, *Phys. Stat. Sol. (c)* **2**, 2141 (2005).
- [48] K. Saarinen, T. Laine, S. Kuisma, J. Nissilä, P. Hautojärvi, L. Dobrzynski, J. M. Baranowski, K. Pakula, R. Stepniewski, M. Wojdak, A. Wyszomolek, T. Suski, M. Leszczynski, I. Grzegory, and S. Porowski, *Phys. Rev. Lett.* **79**, 3030 (1997).
- [49] E. Calleja, M. A. Sánchez-García, D. Basak, F. J. Sánchez, F. Calle, P. Youinou, E. Muñoz, J. J. Serrano, J. M. Blanco, C. Villar, T. Laine, J. Oila, K. Saarinen, P. Hautojärvi, C. H. Molloy, D. J. Somerford, and I. Harrison, *Phys. Rev. B* **58**, 1550 (1998).
- [50] P. Laukkanen, S. Lehtonen, P. Uusimaa, M. Pessa, J. Oila, S. Hautakangas, K. Saarinen, J. Likonen, and J. Keränen, *J. Appl. Phys.* **92**, 786 (2002).
- [51] T. Zywiets, J. Neugebauer, and M. Scheffler, *Appl. Phys. Lett.* **73**, 487 (1998).
- [52] A. L. Rosa, J. Neugebauer, J. E. Northrup, C. D. Lee, and R. M. Feenstra, *Appl. Phys. Lett.* **80**, 2008 (2002).
- [53] A. J. Ptak, T. H. Myers, L. S. Hirsch, L. T. Romano, C. G. Van de Walle, and J. E. Northrup, *Appl. Phys. Lett.* **78**, 285 (2001).
- [54] T. Mattila and R. M. Nieminen, *Phys. Rev. B* **55**, 9571 (1997).
- [55] J. Neugebauer and C. Van de Walle, *Appl. Phys. Lett.* **69**, 503 (1996).
- [56] K. Saarinen, T. Suski, I. Grzegory, and D. C. Look, *Phys. Rev. B* **64**, 233201 (2001).
- [57] J. Oila, V. Ranki, J. Kivioja, K. Saarinen, P. Hautojärvi, J. Likonen, J. M. Baranowski, K. Pakula, T. Suski, M. Leszczynski, and I. Grzegory, *Phys. Rev. B* **63**, 045205 (2001).
- [58] A. Uedono, S. F. Chichibu, Z. Q. Chen, M. Sumiya, R. Suzuki, T. Ohdaira, T. Mikado, T. Mukai, and S. Nakamura, *J. Appl. Phys.* **90**, 181 (2001).